Thermomechanical fatigue and creep of turbine housing of turbocharger: Damage operator approach

Michal Bartošák*[1], Miroslav Španiel[1]

[1]ČVUT v Praze, Fakulta strojní, Ústav mechaniky, biomechaniky a mechatroniky, Technická 4, 166 07 Praha 6, Česká republika

Abstract

A damage operator approach for non-isothermal loading is applied for lifetime calculation of the thermomechanically loaded turbine housing of a turbocharger. Combination of thermomechanical fatigue and creep is considered, oxidation is taken into account indirectly. Results from transient thermal and structural FEA have been transferred to C++ post-processing program and both fatigue and creep damage predicted. Critical zones corresponding to the loading are identified.

Key-words: thermomechanical fatigue; creep; kinematic hardening; hysteresis operator; continuous rainflow method; strain-life approach

1. Introduction

Turbine housing of the turbocharger provides kinetic energy, needed for charging, using remaining enthalpy of the exhaust gas. The component operates usually below 600°C, but temperature can exceed up to 800°C. Inhomogeneous distribution of temperature and boundary conditions of the component constrains thermal expansion, resulting in inelastic strains and stresses. This is termed termomechanical fatigue (TMF). At high temperature, creep or relaxation occurs and time dependent plasticity significantly affects lifetime and cannot be neglected. This all is due to variable service conditions, which usually contains start up, load, partial load and shutdown [1]. Operating status for the investigated component is nearly cyclically stable.

Main damage mechanisms for components operating at high temperatures are fatigue, oxidation and creep [2]. Creep becomes significant especially at high temperature and for long dwell periods. It's also known, that fatigue and creep damage could be treated separately. Enviromental effect could be also separated [3]. In this case, oxidation is taken into account indirectly, as test were performed under ambient conditions and not in a vacuum. Fatigue and creep damage is computed separately, based on Palmgren-Miner linear accumulation rule.

Thermal and structural finite element analysis (FEA) is a must for a lifetime prediction of the components subjected to thermomechanical fatigue [4]. Temperature field can result from steady-state or transient analysis. Structural FEA can be either elastic, elastoplastic or viscoplastic.

The aim of this paper is to present a damage operator approach (DOA) application [5, 6, 7] for the turbine housing, based on transient thermal and elastoplastic structural FEA with viscoplastic aproximation as a part of the post-processing step. In the case of DOA, continuous damage calculation is possible for both isothermal [8, 9] and non-isothermal loading [10].

*Corresponding author: michal.bartosak@fs.cvut.cz

2. Material data assessment

Material of the investigated component is Si-Mo 4.06. In terms of elastoplastic material data identification, isothermal LCF tests have been attained at 20°C, 400°C, 550°C, 650°C and 750°C; as symmetric triangular shaped cycles at constant strain rate $\dot{\epsilon}_{11} = 3.10^{-3}s^{-1}$, no dwell periods, fully reversed ($R_\epsilon = -1$), total strain range $\Delta\epsilon_{11}$ from 0.005 to 0.024. For this strain rate, effect of cyclic creep should be almost excluded.

Viscoplastic material data has been identified from relaxation tests for three selected temperatures (550°C, 650°C ad 750°C) with five-minute hold time at peak strain in tension, for $\Delta\epsilon_{11} = 0.012$.

Creep rupture tests under constant load have been performed at three temperatures and three different stress levels, as creep damage is expected to contribute less than fatigue damage [6].

All experiments have been performed on the test stand in 12105 laboratory [11].

2.1. Elastoplastic material data

Life assessment of high temperature components under cyclic deformation conditions depends on the selected material model. Here, an elastoplastic constitutive model used is used for the FEA. Widely accepted and popular non-linear Chaboche kinematic hardening model has been selected, capable to describe time-independent cyclic plasticity [12, 13]. Incremental formulation of the model is as follows

$$d\boldsymbol{\epsilon} = d\boldsymbol{\epsilon}_e + d\boldsymbol{\epsilon}_{pl} \tag{1}$$

$$\boldsymbol{\sigma} = \boldsymbol{a} : \boldsymbol{\epsilon}_e \tag{2}$$

$$d\boldsymbol{\epsilon}_{pl} = d\lambda \frac{\partial f}{\partial \boldsymbol{\sigma}},\ d\lambda = \sqrt{\frac{2}{3} d\boldsymbol{\epsilon}_{pl} : d\boldsymbol{\epsilon}_{pl}} \tag{3}$$

$$f = \sqrt{\frac{3}{2}(\boldsymbol{\sigma}' - \boldsymbol{\alpha}') : (\boldsymbol{\sigma}' - \boldsymbol{\alpha}')} - \sigma_Y = 0 \tag{4}$$

$$d\boldsymbol{\alpha}_i = \frac{C_i}{\sigma_Y}(\boldsymbol{\sigma} - \boldsymbol{\alpha}) d\lambda - \gamma_i \boldsymbol{\alpha}_i d\lambda + \frac{1}{C_i}\frac{\partial C_i}{\partial T}\boldsymbol{\alpha}_i dT \tag{5}$$

$$d\boldsymbol{\alpha}_i = \sum_{i=1}^{m} d\boldsymbol{\alpha}_i. \tag{6}$$

Mechanical strain tensor $d\boldsymbol{\epsilon}$ is a linear combination of reversible elastic part $d\boldsymbol{\epsilon}_e$ and inelastic part $d\boldsymbol{\epsilon}_{pl}$, Eq.(1). Stress tensor $\boldsymbol{\sigma}$ is obtained from the generalized Hooke's law for a linear, elastic and isotropic continuum, Eq.(2), $\boldsymbol{a}$ denotes fourth order elastic tensor. Associated flow rule is assumed, Eq.(3), $d\lambda$ denotes plastic multiplier. Von Mises yield function f is defined in Eq.(4), where $\boldsymbol{\sigma}', \boldsymbol{\alpha}'$ and σ_Y are deviatoric stress tensor, deviatoric backstress tensor and the initial size of yield surface at zero plastic strain, respectively. σ_Y remains constant, as isotropic hardening is neglected, as usual for TMF. Simulated Baushinger effect and anisotropy induced by work hardening correspond to a cyclic loading with continuously reversed direction of plastic strain, this is often caused by the alternating heating up and cooling down phases [6].

Chaboche introduced [12] that the overall backstress is sum of the multiple components, providing accurate description of stress strain response, Eq.(6). Evolution of the backstress component with accumulated plastic strain is defined in Eq.(5) as a superposition of purely kinematic term and a relaxation term $\gamma_i \boldsymbol{\alpha}_i d\lambda$ introduced by Frederick and Armstrong [14]. A temperature dependent term makes stress-strain response independent on temperature history and also states, that material data could be calibrated from isothermal LCF tests. The value of C_i corresponds to initial plastic modulus and C_i/γ_i is the maximum amount of strain hardening occuring for large plastic strains [13].

The number of backstress is usually considered to be 3, with a general rule $C_1 \gg C_2 \gg C_3$ and $\gamma_1 \gg \gamma_2 \gg \gamma_3$. The first term represents large (initial) plastic modulus, the second term corresponds to moderate segment of stress-strain curve. Finally, the third term describes constant hardening observed for large strains [13], Fig. 1.

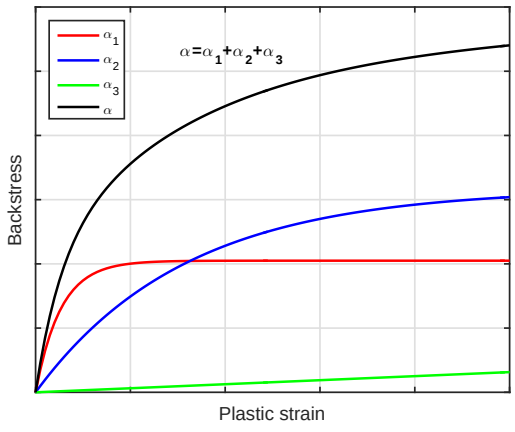

Fig. 1. *Three term backstress superposition.*

Model parameters vary with temperature. Mostly these parameters are calibrated only for the single temperature independently, which cause model parameters to be scattered. Implementation of such scattered data in commercial FE software packages (e.g. ABAQUS and ANSYS) may cause convergence issues. Also, modelling stress-strain trajectory between selected temperatures could be inaccurate. It has been shown recently, that for a narrow range, exponential decay of parameters should be expected[15].

In this paper, model parameters have been calibrated to follow a monotonic downward trend, mathematically described as a Boltzmann function for the temperature range 20-750°C. Temperature dependent Young modulus E is assumed to decrease exponentialy, Eq.(10). Three backstress components are used for stress-strain curve description, γ_3 is assumed to be zero. Parameters change with temperature can be written as follows

$$C_{1-3}(T) = \frac{a_{01-03} - a_{04-06}}{1 + exp(\frac{T - a_{07}}{a_{08}})} + a_{04-06} \tag{7}$$

$$\gamma_{1-2}(T) = \frac{b_{01-02} - b_{03-04}}{1 + exp(\frac{T - b_{05}}{b_{06}})} + b_{03-04} \tag{8}$$

$$\sigma_Y(T) = \frac{c_{01} - c_{02}}{1 + exp(\frac{T - c_{03}}{c_{04}})} + c_{02} \tag{9}$$

$$E(T) = d_{01}(1 - d_{02} \exp \frac{T}{d_{03}}) \tag{10}$$

where $a_{01-08}, b_{01-06}, c_{01-04}$ and d_{01-03} are the calibrated constants, $T(°C)$ is temperature.

In terms of calibration, five hysteresis loops with total strain range $\Delta\epsilon_{11} = 0.012$ have been selected from isothermal LCF tests. An averaged stress–strain response for each test was assigned by consideration of 15 stabilized hysteresis loops at mid-life. End-life was classically determined when 10% drop in tension load occured. Optimization script has been developed in MATLAB. Principle is to search global minimum of the objective function, which was defined as sum of squares of procentual differences between tested and simulated stress. Initial guesses have been obtained from the analytical solution for each temperature separately. Then the objective function was minimized, so that the hysteresis loops were simulated by the analytical solution. Finally, MATLAB Optimization toolbox was linked with ABAQUS by simple PYTHON script [15]. Calibration model in ABAQUS consists of five elements, each at different (measured) temperature, with kinematic boundary conditions corresponding to the selected strain range. Stabilized solution is obtained with Direct cyclic procedure [16] with 50 Fourier terms. Data of five resampled simulated hysteresis loops are reported by the script to MATLAB and guessed parameters are refreshed, until the defined requirements of the objective function are met.

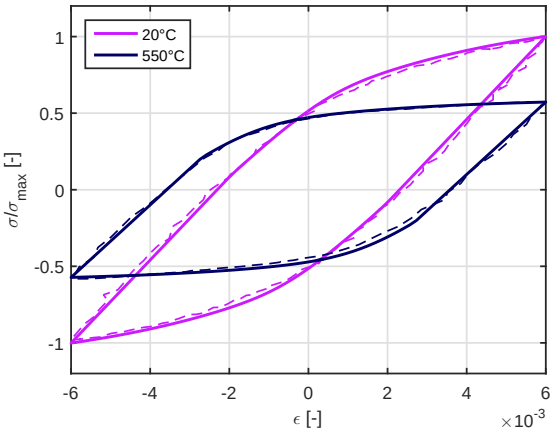

Fig. 2. *Test (thin dashed line) and simulated (thick solid line) cyclically stable hysteresis loops at 20° C and 550° C.*

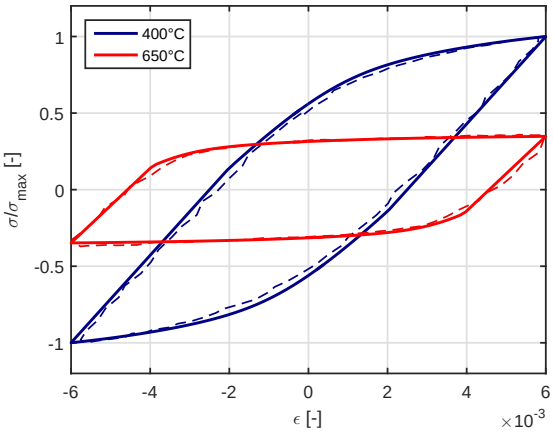

Fig. 3. *Test (thin dashed line) and simulated (thick solid line) cyclically stable hysteresis loops at 400° C and 650° C.*

2.2. Viscoplastic material data

Viscoplastic material data were obtained from isothermal relaxation tests. This should represent steady-state operating phase of the component. Law of perfect viscoplasticity with elastic domain [13, 17] is defined as follows

$$\dot{\epsilon}_{vp}(t) = \langle \frac{\sigma(t) - k(T)}{K(T)} \rangle^{N(T)} \qquad (11)$$

where $K(T)$, $k(T)$ and $N(T)$ are material and temperature dependent data. The McCauley brackets $\langle . \rangle$ are used here to ensure that when $|\sigma(t)| < k(T)$ (inside the elastic domain) $\dot{\epsilon}_{vp}$ cancels out continuously. The expression corresponds to Norton's equation for the secondary creep [18].

Viscoplastic material parameters have been calibrated separately for each temperature, values between test temperatures are obtained by PCHIP.

Constitutive law, Eq.(11), is used in viscoplastic aproximation. If viscoplastic FEA is performed, the constitutive law could be used as a user subroutine or a power-law creep model [16, 18] (without elastic domain, secondary stage creep).

Proposed approach correspond to non-unified (uncoupled) creep-plasticity model.

3. Finite element analysis

The presented approach comprises three steps. In the first step, a temperature field is computed from transient thermal FEA, which is subsequently used in the sedond step, in the structural analysis. Last step includes viscoplastic aproximation and lifetime calculation with the intensive use of Prandtl type hysteresis operators. ABAQUS was chosen for the finite element analysis, for both transient thermal and structural.

The thermal shock test was performed on the gas stand. Extreme temperature gradients are caused by alternating heating-up and cooling down, Fig. 5. Maximum and minimum test temperatures represent full load and partial load, respectively. For the purpose of numerically simulating temperature behaviour of the component, heat transfer coefficients and thermal boundary conditions were calibrated on the basis of the measurements obtained by infrared thermography and thermocouples (M. Nesládek).

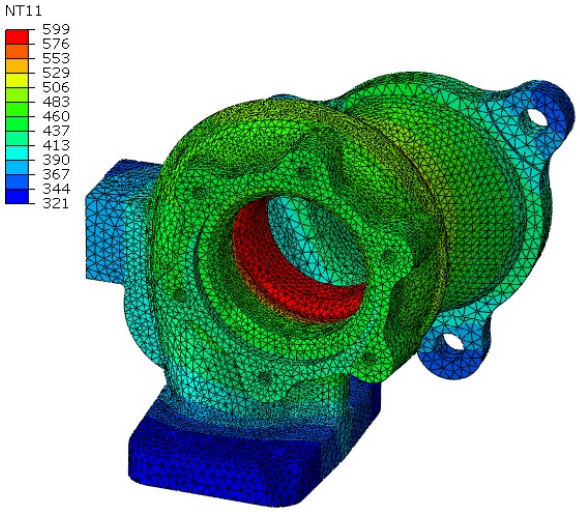

Fig. 4. *Temperature field from the transient thermal FEA for the most heated state.*

Inhomogenous temperature distribution is obtained from the transient thermal analysis from the previous step. The mechanical boundary conditions result from the mounting of the system. In general, change in temperature of material produces thermal strains, constrained thermal expansion produces stress. The von Mises stress field computed in the structural FEA is presented in Fig. 6.

Elastoplastic FEA model for the structural analysis of the investigated component contains a total of almost 500,000 nodes. In the case of a time dependent DOA, only one thermal shock needs to be perfomed. It takes several hours to perform the analysis.

In the last step, equivalent nodal stress and temperatures are transferred to post-processing program. For this reason, User C/C++ post-processing program [16] has been developed for the ABAQUS, preserving high computation speed and direct access to the output database.

Equivalent stresses are obtained by applying the signed von Mises or critical plane approach. The signed von Mises has been selected for this paper.

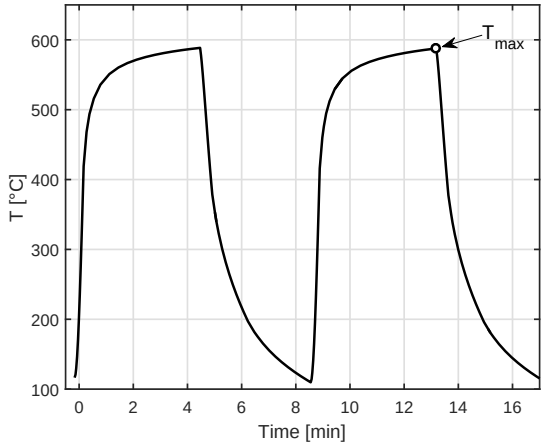

Fig. 5. *Temperature load history of thermal shocks of the component (in the volute).*

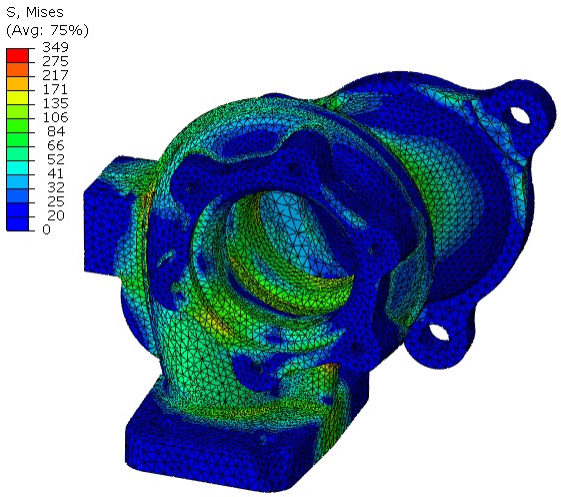

Fig. 6. *Von Mises stress field from structural FEA for the most heated state.*

4. Damage operator based lifetime calculation

4.1. Fatigue damage

The rainflow method due to Endo [19] is widely accepted and commonly used. It's used to decompose an arbitrary sequence of load into cycles and to count those cycles, together with Palmgren-Miner linear accumulation rule. In the case of TMF, temperature is changing, this can lead to non-closed load cycles. Thus traditional rainflow counting can be no longer justified. It has been shown, that traditional rainflow counting directly corresponds to the memory structure of the elastoplastic constitutive law [20]. Also, it has been proven, that the total damage through the Palmgren-Miner rule is a continuous functional of the loading history and could be expressed as the total variation of the output of a hysteresis operator [9, 8]. This was eventually extended for non-isothermal cases [10], enabling online fatigue damage calculation.

More details about equations (12)-(27) given below can be found in [5, 6, 7, 10].

The equivalent stress $\sigma_i(t_i)$ and temperature history $T_i(t_i)$ are obtained from elastoplastic FEA with kinematic hardening. First, using the DOA, uniaxial instantenous strain $\epsilon_i(t_i)$ can be expressed in the form of the Prandtl type operator as follows

$$\epsilon_i(t_i) = \sum_{i=1}^{n_r} \alpha_j(T_i)\sigma_{\alpha j}(t_i) \tag{12}$$

for $0 \leqslant t_1 \leqslant t_2 \leqslant ... \leqslant t_i \leqslant ...$, where T_i is a current temperature and $\sigma_{\alpha j}$ is the play operator with general initial value given as follows

$$\sigma_{\alpha j}(t_i) = max\{\sigma_i(t_i) - r_j, min\{\sigma_i(t_i) + r_j, \frac{\alpha_j(T_{i-1})}{\alpha_j(T_i)}\sigma_{\alpha j}(t_{i-1})\}\}. \tag{13}$$

$\sigma_{\alpha j}(t_i)$ is the backstress and follows kinematic hardening, r_j are yield stresses of the segment sliders, $\alpha_j(T_k)$ are temperature dependent Prandtl densities and can be derived explicitly as follows

$$\alpha_j(T_k) = \frac{1}{r_{j+1} - r_j}(\epsilon_{ij+1}(T_k) - \sum_{i=1}^{j-1} \alpha_i(T_k)(r_{j+1} - r_i)) \tag{14}$$

in the temperature range $k = 1, ..., n_T$ and for segments $j = 1, ..., n_r$. Values are obtained from material and temperature dependent $\sigma_i - \epsilon_i$ cyclically stable cyclic stress-strain curves, Fig. 7. Cyclic stress-strain curves could be derived from Chaboche model parameters or directly from LCF tests. Here, Ramberg-Osgood relation [21] is chosen as a decription of cyclic stress-strain curve. Model parameters have been derived from LCF tests directly and calibrated similarly to the backstresses in Section 2.

This stage of the model can be interpreted as a serially connected stress controlled spring-slider model and corresponds to time-independent constitutive law.

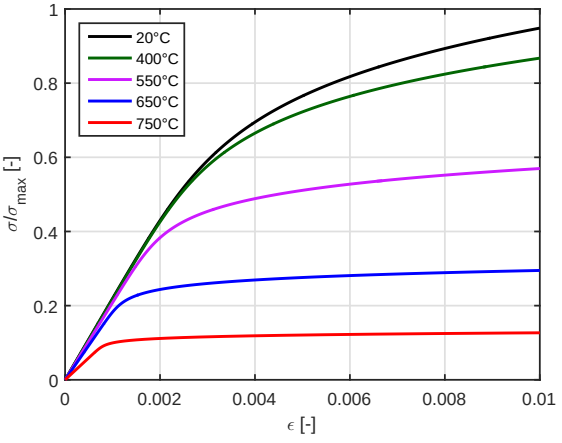

Fig. 7. *Cyclically stable cyclic stress-strain curves for the Si-Mo 4.06.*

The next part is dedicated to the calculation of the viscoplastic strain. The true stress $\sigma(t_{i-1})$ and instantenous strain $\epsilon_i(t_i)$ are assumed to remain constant in the time step $(t_i - t_{i-1})$. The viscoplastic strain is obtained as follows

$$\epsilon_{vp}(t_i) \approx \; sgn(\sigma(t_{i-1})) \cdot \langle \frac{|\sigma(t_{i-1})| - k(T_{i-1})}{K(T_{i-1})} \rangle^{N(T)} \cdot \; (15)$$
$$\cdot f \cdot (t_i - t_{i-1}) + \epsilon_{vp}(t_{i-1}).$$

A multiplier f is added in order to avoid viscous strain discontinuity at the creep temperature $T_c = 450°C$. The multiplier is defined as follows

$$f = \begin{cases} exp(\frac{T_{i-1} - T_{min}}{T_{i-1} - T_c}), & T_c \leqslant T_{i-1} \leqslant T_{min} \\ 1.00, & T_{min} \leqslant T_{i-1} \end{cases} \quad (16)$$

where T_{min} is minimum test temperature (550°C). The multiplier makes the viscous strain continuously decay as the temperature decreases to T_c. There is no creep for $T_{i-1} < T_c$. Better accuracy could be achieved by adding an additional subdivision of time.

In the next step, instantenous strain $\epsilon_i(t_i)$ is converted into the true stress $\sigma(t_i)$ and elastoplastic strain $\epsilon_{ep}(t_i)$, using non-linear strain controlled Maxwell model, Fig. 8. Elastoplastic strain is obtained as follows

$$\epsilon_{ep}(t_i) = \begin{cases} \epsilon_i(t_i) - \epsilon_{vp}(t_i), & T_c \leqslant T_{i-1} \\ \epsilon_i(t_i) - \epsilon_{vp}(t_{i-1}), & T_{i-1} \leqslant T_c. \end{cases} \quad (17)$$

True stress is obtained from the strain controlled spring-slider model, from all segments as

$$\sigma(t_i) = \sum_{i=1}^{n_q} \beta_j(T_i)\epsilon_{\beta j}(t_i) \quad (18)$$

for $0 \leqslant t_1 \leqslant t_2 \leqslant ... \leqslant t_i \leqslant ...$, where T_i is the current temperature and $\epsilon_{\beta j}$ is the play operator with general initial value given as follows

$$\epsilon_{\beta j}(t_i) = max\{\epsilon_{ep}(t_i) - q_j, min\{\epsilon_{ep}(t_i) + q_j, \frac{\beta_j(T_{i-1})}{\beta_j(T_i)}\epsilon_{\beta j}(t_{i-1})\}\}. \quad (19)$$

where $\epsilon_{\beta j}(t_i)$ is the backstrain, q_j are yield strains of the segment sliders, the spring stifness $\beta_j(T_k)$ are temperature dependent Prandtl densities and can be derived explicitly as follows

$$\beta_j(T_k) = \frac{1}{q_{j+1} - q_j}(\sigma_{j+1}(T_k) - \sum_{i=1}^{j-1} \beta_i(T_k)(q_{j+1} - q_i)) \quad (20)$$

and can be obtained from cyclically stable cyclic stress-strain curves.

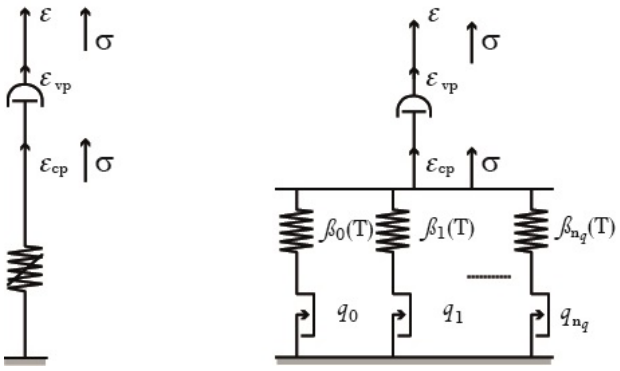

Fig. 8. *Strain-controlled non-linear Maxwell model [7].*

If the viscoplastic FEA is performed, the true stress is obtained from FEA and viscoplastic aproximation is superfluous.

At this time, true stress $\sigma(t_i)$ and elastoplastic strain $\epsilon_{ep}(t_i)$ are transferred to chosen damage parameter. Following options have been selected. No mean stress correction

$$P(t_i) = \epsilon_{ep}(t_i) \quad (21)$$

and Smith-Watson-Topper parameter [22]

$$P(t_i) = P_{SWT}(t_i) = \sqrt{(\sigma_m(t_i) + \sigma_a(t_i))E(T_i)\epsilon_a^{ep}(t_i)}. \quad (22)$$

P_{SWT} requires online signal decomposition into the mean stress and stress and strain amplitude, details can be found in [23].

Fatigue damage is expressed as a total variation

$$D_f(t_i) = D_f(t_{i-1}) + |\mathcal{D}(t_i) - \mathcal{D}(t_{i-1})|. \quad (23)$$

Damage operator $\mathcal{D}(t_i)$ represents the cyclic damage evolution, Fig. 9., and is expressed as follows

$$\mathcal{D}(t_i) = \sum_{j=1}^{n_p} \mathcal{D}_j(t_i) = \sum_{j=1}^{n_p} \gamma_j(T_i)P_{\gamma_j}(t_i) \quad (24)$$

for $0 \leqslant t_1 \leqslant t_2 \leqslant ... \leqslant t_i \leqslant ...$, where T_i is a current temperature and $P_{\gamma j}$ is the play operator with general initial value given as follows

$$P_{\gamma_j}(t_i) = max\{P(t_i) - p_j, min\{P(t_i) + p_j, \frac{\gamma_j(T_{i-1})}{\gamma_j(T_i)}P_{\gamma_j}(t_{i-1})\}\}. \quad (25)$$

$P_{\gamma_j}(t_i)$ represents backstress and follows kinematic hardening, p_j are yield stresses of the segment sliders, $\gamma_j(T_k)$ are temperature dependent Prandtl densities and can be derived explicitly as follows

$$\gamma_j(T_k) = \frac{1}{p_{j+1} - p_j}(\frac{d_{fj+1}(T_k)}{4} - \sum_{i=1}^{j-1} \gamma_i(T_k)(p_{j+1} - p_i)). \quad (26)$$

Values of $\gamma_j(T_k)$ are obtained from temperature dependent fatigue curves from LCF tests. Fatigue curves need to be first transformed from the $P - N_f$, Fig. 10., to the corresponding $P - d_f$ curves

$$d_f = \frac{1}{N_f}. \quad (27)$$

Damage operator represents cyclic fatigue damage evolution and follows Masing and memory rules.

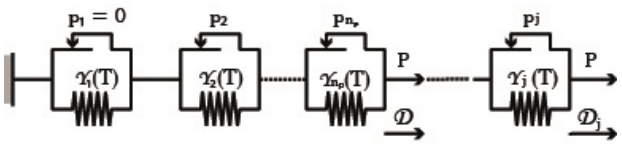

Fig. 9. *The Prandtl damage operator in the form of the spring-slider model [10].*

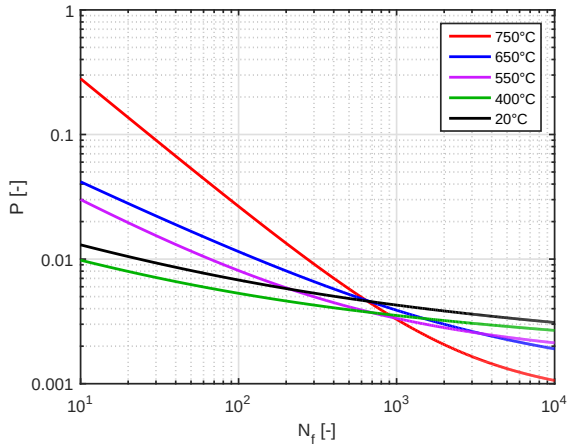

Fig. 10. *P-N_f for the Si-Mo 4.06.*

4.2. Creep damage

For a known uniaxial true stress and temperature, creep damage D_c is computed using Robinson's rule (time-fraction rule) as follows

$$D_c(t_i) = \frac{\Delta t_i(\sigma_i, T_i)}{t_{ri}(\sigma_i, T_i)} + D_c(t_{i-1}) \tag{28}$$

where Δt_i is time under current loading conditions and t_{ri} is corresponding time to the rupture for the same loading conditions, Fig. 11. Test were performed only for limited number of samples. Missing values are assessed by a time-temperature parameter. Restrained Manson-Brown parameter(RMB), proposed in [24], is used for the calculation

$$RMB = \frac{log\ t_{ri} - log\ t_a\ T_i^{|q|-1}}{(T_i - T_a\langle q\rangle)^q}. \tag{29}$$

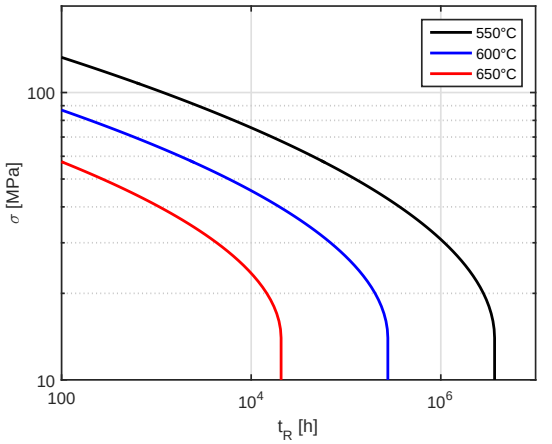

Fig. 11. *Creep rupture curves for the Si-Mo 4.06.*

Second degree polynomial is usually sufficient to describe the stress function

$$RMB = a_0(T_i) + a_1(T_i)log\ \sigma_i + a_2(T_i)log^2\ \sigma_i. \tag{30}$$

The coefficients a_0, a_1, a_2, $log\ t_a$, q and T_a are obtained by least square method from the creep rupture test data.

For each time step, RMB coefficients are transferred to the second degree polynomial as follows

$$log\ t_{ri} = b_0(T_i) + b_1(T_i)log\ \sigma_i + b_2(T_i)log^2\ \sigma_i. \tag{31}$$

Maximal correlation coefficient has been obtained for $q = 1$ in this study. That correspond to the Manson–Haferd parameter. Tensile-compressive creep is assumed.

4.3. Total damage

Total damage at time t_i can be obtained as follows

$$D(t_i) = D_f(t_i) + D_c(t_i). \tag{32}$$

The assumed loading history should be doubled to obtain a "stabilization" of the computed damage. Total damage of the first run is computed as follows

$$D_1 = D_{1f} + D_{1c} \tag{33}$$

and total damage of the following runs as

$$D_2 = D_{2f} + D_{2c}. \tag{34}$$

The predicted number of cycles to failure (initiation of a crack growth) is obtained as follows

$$N_f = \frac{1 - D_1 + D_2}{D_2}. \tag{35}$$

In the case of $D_1 \geq 1$ then $N_f = 1$. Limit damage value is assumed to be 1.

Fig. 12. demonstrates simulated critical zones for the turbine housing of the turbocharger. Smith-Watson-Topper mean stress corection, tensile-compressive creep and signed von Mises stress are assumed for the lifetime calculation. The number of segments used is 150 ($n_r = n_q = n_p = 150$).

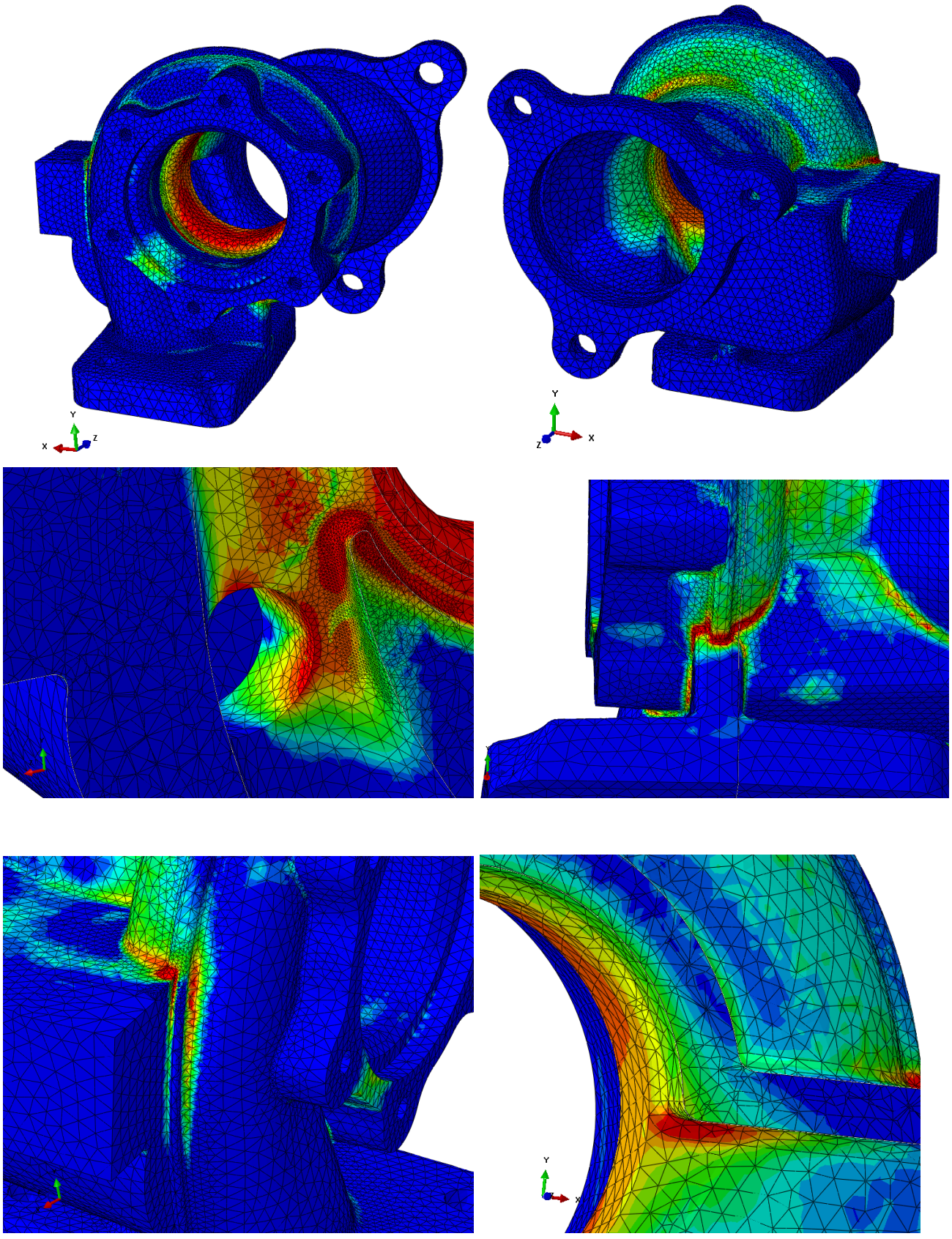

Fig. 12. *The selected simulated critical zones for the turbine housing of the turbocharger.*

5. Conclusions

Critical zones for the turbine housing of the turbocharger have been identified according to the simulated thermomechanical loading. Proposed elastoplastic material model with kinematic hardening is capable of describing time independent behaviour of the component. Viscoplastic approximation enables fast computation of viscous strain using hysteresis operators, comprising speed and accuracy. A damage operator enables continuous damage calculation, which is especially suited for the thermomechanical fatigue.

Future research will be dedicated especially to viscoplasticity modelling and temperature dependent multiaxial criterion. Also other types of loading cycles are planned to be simulated on the turbine housing of the turbocharger. Finally the results should be verified experimentally by either partial destruction or total destruction of the component on the test stand.

The presented approach is implemented as User C/C++ post-processing program for ABAQUS. Identification of the time-temperature and elastoviscoplastic material parameters is implemented in the form of a script in PYTHON and MATLAB.

All experiments have been performed on the new test stand in 12105 laboratory [11], which has proven to meet the requirements.

Developed software can be extended by notch formula enabling fast computations from elastic FEA. This can provide significant acceleration in the phase of design calculations in industry.

Acknowledgement

The authors would like to acknowledge support from Technology Agency of the Czech Republic, grant No. TE01020020, and support from the Grant Agency of the Czech Technical University in Prague, grant No. SGS15/187/OHK2/3T/12.

Nomenclature

$\boldsymbol{a}$	elastic modulus tensor (MPa)
C_i	initial hardening modulus (MPa)
D_c	creep damage (1)
D_f	fatigue damage (1)
d_f	cycle damage (1)
$d\boldsymbol{\alpha_i}$	backstress term rate (MPa)
$d\boldsymbol{\epsilon}$	mechanical strain rate tensor (−)
$d\boldsymbol{\epsilon}_e$	plastic strain rate tensor (−)
$d\boldsymbol{\epsilon}_{pl}$	plastic strain rate tensor (−)
$d\lambda$	plastic multiplier (−)
E	elastic modulus (MPa)
f	yield function (MPa)
K	material parameter in the viscoplastic law (MPa)
k	elastic limit (MPa)
N	exponent in the viscoplastic law (−)
N_f	cycles to failure (−)
$P(t_i)$	damage parameter (−)
$P_{\gamma j}$	the play operator (−)
p_j	fictive yield of damage parameter (−)
q_j	fictive yield strain (−)
r_j	fictive yield stress (MPa)
T	temperature (°C, K)
t, t_i	time (s)
t_{ri}	rupture time (h, s)
$\boldsymbol{\alpha_i}$	backstress term (MPa)
α_j	the Prandtl density (MPa^{-1})
β_j	the Prandtl density (MPa)
ϵ_a^{ep}	elastoplastic strain amplitude (−)
ϵ_{ep}	elastoplastic strain (−)
ϵ_i	instantenous strain (−)
$\epsilon_{\beta j}$	the play operator (−)
ϵ_{vp}	viscous strain (−)
$\dot{\epsilon}_{vp}$	viscous strain rate (−)
γ_i	part of the relaxation term of the backstress (−)
γ_j	the Prandtl density (−)
$\boldsymbol{\sigma}$	stress tensor (MPa)
$\boldsymbol{\sigma'}$	deviatoric part of stress tensor (MPa)
σ_a	stress amplitude (MPa)
$\sigma_{\alpha j}$	the play operator (MPa)
σ_m	mean stress stress (MPa)
σ_i	equivalent stress from FEA (MPa)
σ_Y	yield stress (MPa)
$\sigma(t_i)$	true stress (MPa)
$\mathcal{D}(t_i)$	the Prandtl damage operator (1)

References

[1] J Granacher, A Scholz, and H Möhlig. "Behaviour of heat resistant power plant steels undergoing variable long term loading conditions". In: *Materialwissenschaft und Werkstofftechnik* 31.1 (2000), pp. 29–37.

[2] Changan Cai et al. "Recent developments in the thermomechanical fatigue life prediction of superalloys". In: *J. Mater.-e,(JOM-e)* (1999), pp. 51–4.

[3] Huseyin Sehitoglu. "Thermo-mechanical fatigue life prediction methods". In: *Advances in fatigue lifetime predictive techniques*. ASTM International, 1992.

[4] Andrei Constantinescu et al. "A computational approach to thermomechanical fatigue". In: *International Journal of fatigue* 26.8 (2004), pp. 805–818.

[5] Domen Šeruga et al. "Durability prediction of EN 1.4512 exhaust mufflers under thermomechanical loading". In: *International Journal of Mechanical Sciences* 84 (2014), pp. 199–207.

[6] Marko Nagode, Frank Längler, and Michael Hack. "Damage operator based lifetime calculation under thermo-mechanical fatigue for application on Niresist D-5S turbine housing of turbocharger". In: *Engineering Failure Analysis* 18.6 (2011), pp. 1565–1575.

[7] M Nagode et al. "Damage Operator-Based Lifetime Calculation Under Thermomechanical Fatigue and Creep for Application on Uginox F12T EN 1.4512 Exhaust Downpipes". In: *Strain* 48.3 (2012), pp. 198–207.

[8] Martin Brokate and Jürgen Sprekels. *Hysteresis and phase transitions*. Vol. 121. Springer Science & Business Media, 2012.

[9] Martin Brokate, Klaus Dressler, and Pavel Krejci. "Rainflow counting and energy dissipation for hysteresis models in elastoplasticity". In: *European journal of mechanics A/Solids* 15.4 (1996), pp. 705–737.

[10] Marko Nagode, Michael Hack, and Matija Fajdiga. "Low cycle thermo-mechanical fatigue: damage operator approach". In: *Fatigue & Fracture of Engineering Materials & Structures* 33.3 (2010), pp. 149–160.

[11] M Španiel, C Novotný, and M Dvořák. "Zařízení pro zkoušky nízkocyklové teplotně mechanické únavy". In: *[Funkční vzorek]* (2013).

[12] Jean-Louis Chaboche. "Time-independent constitutive theories for cyclic plasticity". In: *International Journal of plasticity* 2.2 (1986), pp. 149–188.

[13] Jean Lemaitre and Jean-Louis Chaboche. *Mechanics of solid materials*. Cambridge university press, 1994.

[14] Charles O Frederick and PJ Armstrong. "A mathematical representation of the multiaxial Bauschinger effect". In: *Materials at High Temperatures* 24.1 (2007), pp. 1–26.

[15] E Hosseini et al. "Temperature dependent representation for Chaboche kinematic hardening model". In: *Materials at High Temperatures* 32.4 (2015), pp. 404–412.

[16] ABAQUS. *User's manual*. Version 6.14.

[17] JL Chaboche. "A review of some plasticity and viscoplasticity constitutive theories". In: *International Journal of Plasticity* 24.10 (2008), pp. 1642–1693.

[18] Royston Kenneth Penny and Douglas Lewis Marriott. *Design for creep*. Springer Science & Business Media, 2012.

[19] Tatsuo Endo. "Damage evaluation of metals for random on varying loading-three aspects of rain flow method". In: *Proc. 1974 Symp. On MBM*. Vol. 1. 1974, p. 374.

[20] UH Clormann and T Seeger. "Rainflow-HCM. Ein Zählverfahren für Betriebsfestigkeitsnachweise auf werkstoffmechanischer Grundlage". In: *STAHLBAU, DER* 55.3 (1986).

[21] Walter Ramberg and William R Osgood. "Description of stress-strain curves by three parameters". In: (1943).

[22] P Watson and TH Topper. "Fatigue-damage evaluation for mild steel incorporating mean stress and overload effects". In: *Experimental Mechanics* 12.1 (1972), pp. 11–17.

[23] Marko Nagode. "Continuous damage parameter calculation under thermo-mechanical random loading". In: *MethodsX* 1 (2014), pp. 81–89.

[24] Domen Šeruga and Marko Nagode. "Unification of the most commonly used time–temperature creep parameters". In: *Materials Science and Engineering: A* 528.6 (2011), pp. 2804–2811.